PNAS RESEARCH ARTICLE | PHYSIOLOGY

Liver cancer development driven by the AP-1/c-Jun~Fra-2 dimer through c-Myc

Latifa Bakiri[a,b,1], Sebastian C. Hasenfuss[b,2], Ana Guío-Carrión[b,3], Martin K. Thomsen[c], Peter Hasselblatt[d], and Erwin F. Wagner[a,e,1]

Contributed by Erwin F. Wagner; received February 28, 2024; accepted March 26, 2024; reviewed by Carlo M. Croce, Michael Karin, and Joseph Schlessinger

Hepatocellular carcinoma (HCC) is a leading cause of cancer-related death. HCC incidence is on the rise, while treatment options remain limited. Thus, a better understanding of the molecular pathways involved in HCC development has become a priority to guide future therapies. While previous studies implicated the Activator Protein-1 (AP-1) (Fos/Jun) transcription factor family members c-Fos and c-Jun in HCC formation, the contribution of Fos-related antigens (Fra-) 1 and 2 is unknown. Here, we show that hepatocyte-restricted expression of a single chain c-Jun~Fra-2 protein, which functionally mimics the c-Jun/Fra-2 AP-1 dimer, results in spontaneous HCC formation in c-Jun~Fra-2^{hep} mice. Several hallmarks of human HCC, such as cell cycle dysregulation and the expression of HCC markers are observed in liver tumors arising in c-Jun~Fra-2^{hep} mice. Tumorigenesis occurs in the context of mild inflammation, low-grade fibrosis, and Pparγ-driven dyslipidemia. Subsequent analyses revealed increased expression of c-Myc, evidently under direct regulation by AP-1 through a conserved distal 3′ enhancer. Importantly, c-Jun~Fra-2-induced tumors revert upon switching off transgene expression, suggesting oncogene addiction to the c-Jun~Fra-2 transgene. Tumors escaping reversion maintained c-Myc and c-Myc target gene expression, likely due to increased c-Fos. Interfering with c-Myc in established tumors using the Bromodomain and Extra-Terminal motif inhibitor JQ-1 diminished liver tumor growth in c-Jun~Fra-2 mutant mice. Thus, our data establish c-Jun~Fra-2^{hep} mice as a model to study liver tumorigenesis and identify the c-Jun/Fra-2-Myc interaction as a potential target to improve HCC patient stratification and/or therapy.

c-Jun/Fra-2 | AP-1 | HCC | mouse models | c-Myc

Significance

Hepatocellular carcinoma (HCC) is a deadly cancer with limited treatment options. The AP-1 (Activator Protein-1) transcription factor components c-Fos and c-Jun were previously linked to HCC, but the role of Fra proteins was unclear. This study establishes a mouse model for HCC research and reveals that hepatic expression of a c-Jun/Fra-2 dimer induces spontaneous tumors with HCC features. Tumor growth is fueled by dysregulated cell cycle, inflammation, dyslipidemia, and increased c-Myc. Switching off c-Jun~Fra-2 reverts tumor growth, whereas escapers maintain c-Myc, consistent with c-Jun/Fra-2-mediated regulation of c-Myc driving HCC. Blocking c-Myc using a Bromodomain and Extra-Terminal motif inhibitor halts tumor growth. The data suggest that the c-Jun/Fra-2-Myc interaction is pertinent to future clinical studies aimed at improving HCC patient care.

Primary liver cancer is the 6th most commonly diagnosed cancer and the 3rd leading cause of cancer death worldwide. Incidence and mortality are higher among men and in low to moderate income countries (1). Hepatocellular carcinoma (HCC), accounting for 75 to 85% of primary liver cancers, develops in the context of chronic liver diseases, such as hepatitis and/or metabolic dysfunction. HCC is increasingly associated with obesity, insulin resistance, and metabolic syndrome and has limited therapeutic options (2, 3). The signaling pathways most frequently involved in hepatocarcinogenesis include Wnt/β-catenin, mTOR, IL-6 (interleukin-6), TGF-β, Ras, Rb, HGF/c-Met, and IGF1, which converge and modulate the activity of the NF-κB, p53, Stat3, c-Myc, and AP-1 (Activator Protein-1) transcription factors (4–6).

The Jun (c-Jun, JunB, JunD) and Fos (c-Fos, FosB, Fra-1, Fra-2) proteins are components of the dimeric AP-1 transcription factor complex (7). While Jun proteins can form homo- or heterodimers, Fos proteins can only form heterodimers with a Jun protein. The AP-1 dimer combinations that coexist in a given cell/biological context, together with dimer-specific variation in DNA sequence affinity and/or coactivator/repressor recruitment, determine the target genes that are positively or negatively regulated by AP-1. The AP-1 dimer pool is modulated by various signals, such as growth factors, inflammatory cytokines, and mechanical and oxidative stress, and plays important roles in many diseases including cancer (7, 8). In genetically engineered mouse models (GEMMs), liver-specific inactivation of c-Jun revealed its essential role in liver regeneration (9), steatohepatitis (10), hepatocyte survival during acute hepatitis (11), endoplasmic reticulum (ER) stress (12), and liver cancer (13–18). In HCC, c-Jun promotes the survival of diethylnitrosamine (DEN)-induced preneoplastic hepatocytes by repressing c-Fos expression (16), while c-Fos is needed for DEN-induced hepatocarcinogenesis when the *c-jun* gene is intact (19). Furthermore, doxycycline (Dox)-switchable c-Fos expression in adult hepatocytes (c-Fos^{hep}) leads to reversible liver inflammation, accumulation of toxic oxysterols and bile acids, activation of the DNA damage response, premalignant transformation, and enhanced DEN-induced HCC (19). The hepatic functions of the other Jun and Fos proteins are less studied, especially in cancer.

Reviewers: C.M.C., The Ohio State University; M.K., University of California, San Diego School of Medicine; and J.S., Yale University.

The authors declare no competing interest.

[1]To whom correspondence may be addressed. Email: latifa.bakiri@meduniwien.ac.at or erwin.wagner@meduniwien.ac.at.

[2]Present address: Beam Therapeutics, Cambridge, MA02142, USA.

[3]Present address: National Center for Cardiovascular Research, 28029, Madrid, Spain.

This article contains supporting information online at https://www.pnas.org/lookup/suppl/doi:10.1073/pnas.2404188121/-/DCSupplemental.

Published April 24, 2024.

Hepatocyte-specific JunB inactivation increases liver damage during acute hepatitis, an effect that is largely counteracted by the proinflammatory role of JunB in hepatic NK/NKT cells (20). JunD knock-out mice are protected from chemically induced liver fibrosis (21) and high fat diet (HFD)-induced hepatosteatosis (22). On the other hand, loss of Fra-1 sensitizes, while hepatic Fra-1, but not Fra-2, expression protects from acetaminophen-induced liver damage, an acute liver failure paradigm (23). Interestingly, Fra-1 and Fra-2 play redundant functions in hepatic lipid metabolism: Fra-1 or Fra-2 expression in hepatocytes prevented and could even revert HFD-induced hepatosteatosis by suppressing the transcription of the nuclear receptor PPARγ, a central regulator of lipid metabolism, while single inactivation of either of the two genes had no effect (22, 24). In contrast, c-Fos activated hepatic *Pparg* transcription, while it suppressed another nuclear receptor LXRα, responsible for increased hepatic cholesterol and oxysterols (19, 22). Thus, Fos-related antigens 1 and 2 (Fra-1/2)- and c-Fos-containing AP-1 dimers exert antagonistic effects on the *pparg2* promoter and lipid handling in the liver. When selected Jun and Fos monomers were tethered by a flexible polypeptide to force specific AP-1 pairing in a "single-chain" approach (25), and expressed in Dox-switchable AP-1^{hep} mice, c-Jun~Fra-2 dimers inhibited, whereas c-Jun~c-Fos, JunB~c-Fos, and JunD~c-Fos dimers activated PPARγ expression and signaling (22, 24).

In this study, we show that hepatic expression of c-Jun~Fra-2 dimers results in spontaneous and reversible HCC formation, while mice expressing Fra-1/2 monomers or c-Jun~Fra-1 dimers remained tumor-free. c-Jun~Fra-2 dimers promote tumorigenesis in murine and human liver cells, in significant part through direct transcriptional activation of *c-myc* expression. Furthermore, we show that established tumors are largely addicted to c-Jun~Fra-2 and sensitive to JQ-1, a Bromodomain and Extra-Terminal motif inhibitor (BETi) that inhibits c-Myc activity.

Results

Spontaneous Liver Tumors in c-Jun~Fra-2^{hep} Mice. Jun~Fra-2^{hep} mice had a shorter lifespan compared to controls, with a median survival of 45 wk after switching on the transgene (*SI Appendix*, Fig. S1*A*). Mutant and control littermates were killed at different time points after transgene induction, which was always started at weaning by Dox removal. All time points indicated hereafter are posttransgene induction. Macroscopically visible liver tumors were observed at 9 mo (Fig. 1*A*), while increased liver to body weight ratio was already apparent at 2 mo (*SI Appendix*, Fig. S1*B*). Nodule number and size was variable (*SI Appendix*, Fig. S1*C*), but the phenotype was highly penetrant, with almost 90% of Jun~Fra-2^{hep} mice having at least one macroscopically visible tumor nodule at 9 mo (*SI Appendix*, Fig. S1*D*). Notably, Fra-1^{hep}, Fra-2^{hep}, and Jun~Fra-1^{hep} mice expressing Fra-1/2 monomers (23) or Jun~Fra-1 dimers, generated with a similar strategy (see *Materials and Methods* and *SI Appendix*, Fig. S7) and kept up to 15 mo off Dox never or rarely developed liver tumors (*SI Appendix*, Fig. S1*D*). Histologically, hyperplastic nodules, adenoma, and HCC were identified in Jun~Fra-2^{hep} liver sections (Fig. 1*A*), while the HCC biomarker (26) "Protein-induced-by-vitamin-K-absence-or-antagonist-II" (PIVKA), was increased in Jun~Fra-2^{hep} sera at 9 mo (Fig. 1*B*). Alpha-fetoprotein (AFP), a more commonly used HCC biomarker, was elevated in the serum of Jun~Fra-2^{hep} mice as early as 1 mo (Fig. 1*C*), but not in aged Fra-1^{hep}, Fra-2^{hep} of Jun~Fra-1^{hep} mice (*SI Appendix*, Fig. S1*E*). AFP was also detected by IHC (immunohistochemistry) in Jun~Fra-2^{hep} liver tumors (Fig. 1*D*). IHC-positivity for "minichromosome-maintenance-complex-component-2" (Mcm2) and Sox9, which have been associated with HCC development and Sorafenib resistance (27–29), was also observed in the tumors (Fig. 1*D*). Hypoalbuminemia (*SI Appendix*, Fig. S1*F*), increased alanine (ALT) and aspartate (AST) aminotransferases as well as alkaline phosphatase (ALP) (*SI Appendix*, Fig. S1*G*) were also observed in Jun~Fra-2^{hep} mice, consistent with early onset liver dysfunction and damage.

Macroscopically visible liver tumors were dissected from Jun~Fra-2^{hep} mice at 9 mo, together with small liver pieces from areas that appeared macroscopically tumor-free, hereafter termed "nontumoral" (NT), and compared to livers of control littermates by RNA and protein analyses. qRT-PCR revealed increased mRNA expression of oncofetal (*h19*, *nope*, *dlk1, bex1*), cancer cell stemness (*cd133, cd44, sox9*), HCC (mcm2, gp73, ly6d), and replicative senescence (p16) markers in Jun~Fra-2^{hep} tumors and NT areas (Fig. 1*E*). Increased Gp73 and Bex was confirmed by immunoblotting (Fig. 1*F*). Activation of ER stress with increased PERK and eIF2a phosphorylation and Bip protein expression was also evident in Jun~Fra-2^{hep} tumoral and NT extracts compared to control livers (*SI Appendix*, Fig. S1*H*). Increased p53, p21, and S139-phosphorylation of histone H2AX (γH2AX), a surrogate marker of DNA damage, as well as decreased p19 were consistent with aberrant cell cycle and replicative stress (Fig. 1*G* and *SI Appendix*, Fig. S1*I*). Overall, most of the molecular changes observed in the tumors were also seen in the NT areas indicating that these areas are likely preneoplastic. Consistently, p21-and γH2AX-positive hepatocytes and increased *p21, p16,* and *p53* mRNA were already apparent in the livers of Jun~Fra-2^{hep} mice at 2 mo (Fig. 1*H* and *SI Appendix*, Fig. S1 *I* and *J*).

Enhanced Proliferation and Moderate Inflammation in c-Jun~Fra-2^{hep} Livers. Genome-wide transcription profiling by RNAseq was performed on 2- and 9-mo liver samples (GSE261005)(30). Unsupervised principal-component analysis (PCA) clearly separated the samples along PC1 and PC2 according to genotype and age, respectively (Fig. 2*A*). Interestingly, while tumoral samples also separated from NT along PC2, the two tumors isolated from the same mouse appeared more distant from each-other than the two tumors isolated from different mice, consistent with intertumoral heterogeneity (Fig. 2*A*). Gene set enrichment analysis [GSEA (31)] revealed enrichment in MSigDB Hallmarks gene sets related to cell cycle, p53 pathway, cell death, and hypoxia in the 3 mutant groups, when compared to their respective control littermates (*SI Appendix*, Fig. S2*A*). CIBERSORTx (32) computational deconvolution at 2 mo using a murine hepatocyte matrix (33) indicated perturbed liver zonation, with increased Zone 2 and undetectable Zone 3 hepatocytes (*SI Appendix*, Fig. S2*B*), which was confirmed by diffuse pericentral Glutamine synthetase IHC positivity in mutants (*SI Appendix*, Fig. S2*C*). The mean expression profile of the 4 tumors relative to control livers was next compared by GSEA with a collection of human and murine liver cancer signatures. A significant correlation was observed with HCC gene signatures, in particular those associated with poor outcome, such as Hoshida subclass S1 (34), Boyault subclass G3 (35), Woo cancer recurrence (36), the hepatoblast subtype of human HCC with prominent AP-1 (37) and pediatric hepatoblastoma with upregulated Myc signaling (38) (Fig. 2*B*). These gene signatures are all characteristic of dedifferentiation, fetal liver–like gene expression, high proliferation, and aggressiveness. There was also a good correlation with murine liver cancer signatures (39), in particular those arising in mice expressing a Myc transgene (Fig. 2*B*). Increased proliferation and altered cell cycle was confirmed by Ki67 and Cyclin D1 IHC (Fig. 2 *C* and *D*) as well as immunoblot and qRT-PCR for a panel of cyclins and Cdks (*SI Appendix*, Fig. S2 *D* and *E*). Increased Cyclin A is consistent with *ccna2* (encoding Cyclin A2) being a direct

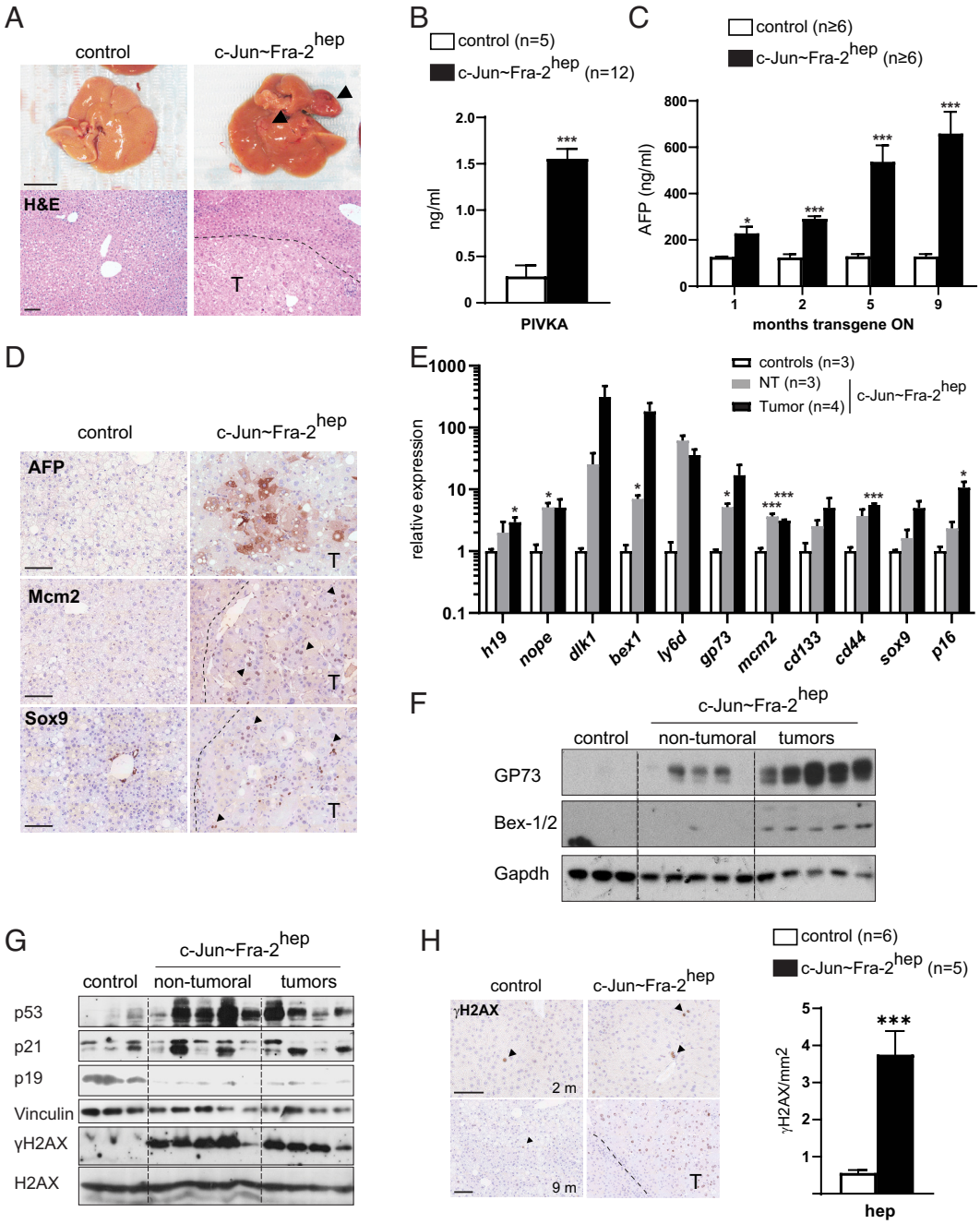

Fig. 1. Liver tumors in c-Jun~Fra-2^{hep} mice. (*A*) Liver morphology and histology in a c-Jun~Fra-2^{hep} and representative control mouse. Bar = 1 cm (*Top*) and 100 µm (H&E: Hematoxylin and Eosin, *Bottom*), tumors (T) are indicated by arrows and dotted line. (*B*) Serum PIVKA, also known as des-gamma-carboxy-prothrombin (DCP). (*C*) Serum AFP in c-Jun~Fra-2^{hep} mice and littermate controls over time. (*D*) AFP, Mcm2, and Sox9 IHC in c-Jun~Fra-2^{hep} and control livers. Bar = 100 µm, tumors (T) are indicated by a dotted line and arrows point to positive nuclei. (*E*) qRT-PCR quantification of oncofetal, stemness, and senescence-associated genes in c-Jun~Fra-2^{hep} tumors and nontumoral (NT) liver areas compared to controls. (*F*) Gp73 and Bex immunoblot in livers extract from c-Jun~Fra-2^{hep} mice (nontumoral and tumors) and controls. (*G*) Immunoblot for cell cycle-, replicative stress- and DNA damage-related proteins in liver extracts from c-Jun~Fra-2^{hep} mice (nontumoral and tumors) and controls. (*H*) γH2AX IHC in liver sections of c-Jun~Fra-2^{hep} mice and controls at 2 mo and 9 of transgene expression (*Left*) and quantification of hepatocyte (hep) γH2AX-positivity at 2 mo (*Right*). Bar = 100µm, tumors (T) are indicated by a dotted line and arrows point to positive nuclei. Unless otherwise indicated, all data are from mice with 9 mo of transgene expression (off Dox at weaning). Gapdh and Vinculin are used to control loading. Bars = means ± SEM. *P < 0.05, ***P < 0.001 (t test to controls).

target of the c-Jun/Fra-2 dimer in cultured cells (25). Increased Ki67-positivity was also observed in nonparenchymal, likely immune cells as early as 2 mo (Fig. 2*D*), along with increased *il6* mRNA (*SI Appendix*, Fig. S2*E*). Therefore, the immune and inflammatory profile of Jun~Fra-2^{hep} livers was examined in more detail. A moderate but consistent increase in immune-cell-related marker expression was observed by IHC (Fig. 2*E* and *SI Appendix*, Fig. S2*F*) and qRT-PCR (Fig. 2*F* and *SI Appendix*, Fig. S2*G*). Furthermore, GSEA using human MSigDB C8 liver cell gene sets (40) revealed that Kupffer cell signatures were among the top enriched in mutant Jun~Fra-2^{hep} livers (*SI Appendix*, Fig. S2*H*). Elevated myeloid cell abundance in mutant livers was confirmed by CIBERSORTx deconvolution using a murine matrix (33), and TREM2-positive macrophages, that are high in HCC and associate with poor prognosis (41) were notably increased (Fig. 2*G*).

We next evaluated signaling pathways that could connect inflammation and proliferation. The relative phosphorylation of ERK, JNK, and p38 was not noticeably changed at 9 mo, while

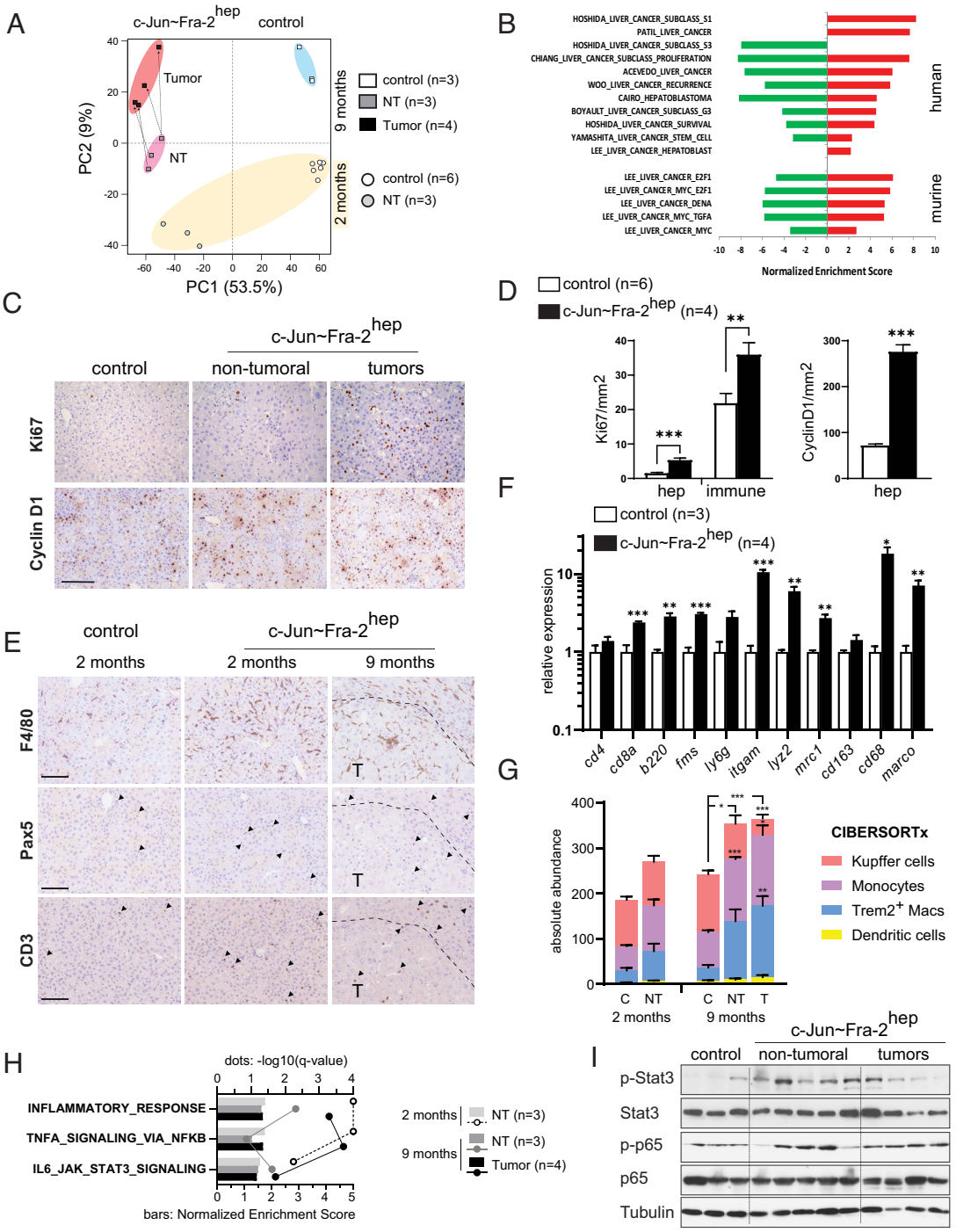

Fig. 2. Phenotypic characterization and inflammation in c-Jun~Fra-2^{hep} livers. (*A*) PCA of RNAseq data. PC1 and PC2 account for 62.5% of sample variability. Individual samples from 2 and 9 mo of transgene expression are depicted with circles and squares, respectively, and the correspondence between NT and tumoral samples from the same mouse indicated with dotted arrows. (*B*) Normalized enrichment scores in c-Jun~Fra-2^{hep} liver tumors relative to controls (RNAseq, n = 3 controls and 4 mutants) compared with human and mouse liver cancer signatures by GSEA. False discovery rate (FDR) q-val < 0.0029 for upregulated (red) and downregulated (green) genes. Data are ordered by FDR in each comparison. (*C*) Ki67 and Cyclin D1 IHC in c-Jun~Fra-2^{hep} liver sections. Bar = 200 µm. (*D*) IHC quantification of Ki67 in hepatocytes (hep) and immune cells (immune) and Cyclin D1 in hepatocytes in liver sections of c-Jun~Fra-2^{hep} mice and controls at 2 mo of transgene expression. (*E*) F4/80 (macrophages), Pax5 (B cells), and CD3 (T cells) IHC in liver sections of c-Jun~Fra-2^{hep} mice and controls. Bar = 100 µm, tumors (T) are indicated by a dotted line and arrows point to positive nuclei. (*F*) qRT-PCR quantification of immune-cell markers in c-Jun~Fra-2^{hep} livers at 2 mo of transgene expression compared to controls. (*G*) CIBERSORTx deconvolution of liver myeloid cells in c-Jun~Fra-2^{hep} liver RNAseq datasets at 2 (control: C, n = 6, mutant: NT, n = 3) and 9 (control: C, n = 3, mutant: NT, n = 3, T: tumors, n= 4) months. (*H*) Top enriched immune-related MSigDB Hallmark signatures in mutant groups compared to their respective controls (RNAseq, 2 mo: n = 6, 9 mo: n = 3) by GSEA. Normalized enrichment scores (NES) are shown as bars and FDR q-values (–log10) as dot plots. Data are ordered by NES in the 2-mo dataset. (*I*) Immunoblot for total and phosphorylated Stat3 and NF-κB p65 in liver extracts from c-Jun~Fra-2^{hep} mice (NT and tumors) and controls. Tubulin is used to control loading. Bars = means ± SEM. *P < 0.05, **P < 0.01, ***P < 0.001 (t test to controls).

PTEN, AKT, and GSK3β phosphorylation was increased to variable extents (*SI Appendix*, Fig. S2*I*). The MSigDB Hallmarks gene sets: Inflammatory response, TNF/NF-κB, and IL6/JAK/STAT3 were enriched in the Jun~Fra-2^{hep} mutant groups (Fig. 2*H*). This is in line with increased relative STAT3 phosphorylation and increased p-STAT3-positive cells at 2 and 9 mo, although the phosphorylation of the p65 NF-κB subunit was not changed (Fig. 2*I* and *SI Appendix*, Fig. S2 *J* and *K*). These results imply

that hepatic Jun~Fra-2 expression leads to cellular and molecular characteristics of malignant transformation in a context of moderate inflammation, even before visible tumors are detected.

Low-Grade Fibrosis and Dyslipidemia in c-Jun~Fra-2^{hep} Livers. Fibrosis and steatosis are often associated with HCC. At 2 mo, Trichrome staining of liver sections (Fig. 3*A*), qRT-PCR (Fig. 3*B*) and WebGestalt (42) overrepresentation of matrix/collagen-related Reactome and Gene Ontology terms (Fig. 3*C*), as well as enrichment in MSigDB C8 hepatic stellate cell signatures (*SI Appendix*, Fig. S2*H*), supported the occurrence of fibrotic events in Jun~Fra-2^{hep} mutant livers. Increased TGFβ signaling was also apparent at 9 mo with increased *tgfb2/tgfbR2* mRNA expression (*SI Appendix*, Fig. S3*A*) and relative Smad2 phosphorylation (Fig. 3*D*). On the other hand, while the epithelial-to-mesenchymal transition MSigDB hallmark gene set was enriched in mutant datasets, lipid/peroxisome metabolism-related hallmarks had negative enrichment scores (*SI Appendix*, Fig. S3*B*), consistent with decreased Oil Red O staining and Pparγ positivity in liver sections (Fig. 3*E*). This is in line with the suppression of Pparγ signaling and HFD-induced NAFLD in c-Jun~Fra-2^{hep} mice (22). Decreased protein and mRNA expression of Pparγ and Pparγ targets were apparent at 2 and 9 mo (Fig. 3*F* and *SI Appendix*, Fig. S3 *C* and *D*). LXR and LXR signaling, driving early preneoplastic events in Fos-expressing mice (19), were not consistently affected in c-Jun~Fra-2^{hep} mice (*SI Appendix*, Fig. S3*E*). Liver triglycerides (Fig. 3*G*), serum triglycerides, and cholesterol (*SI Appendix*, Fig. S3*F*) were also decreased in mutant mice at 9 mo, similar to what was observed after HFD (22). These data indicate that while low-grade fibrosis might contribute to liver cancer development in Jun~Fra-2^{hep} mice, tumors occur in a dyslipidemic context with decreased hepatic lipids.

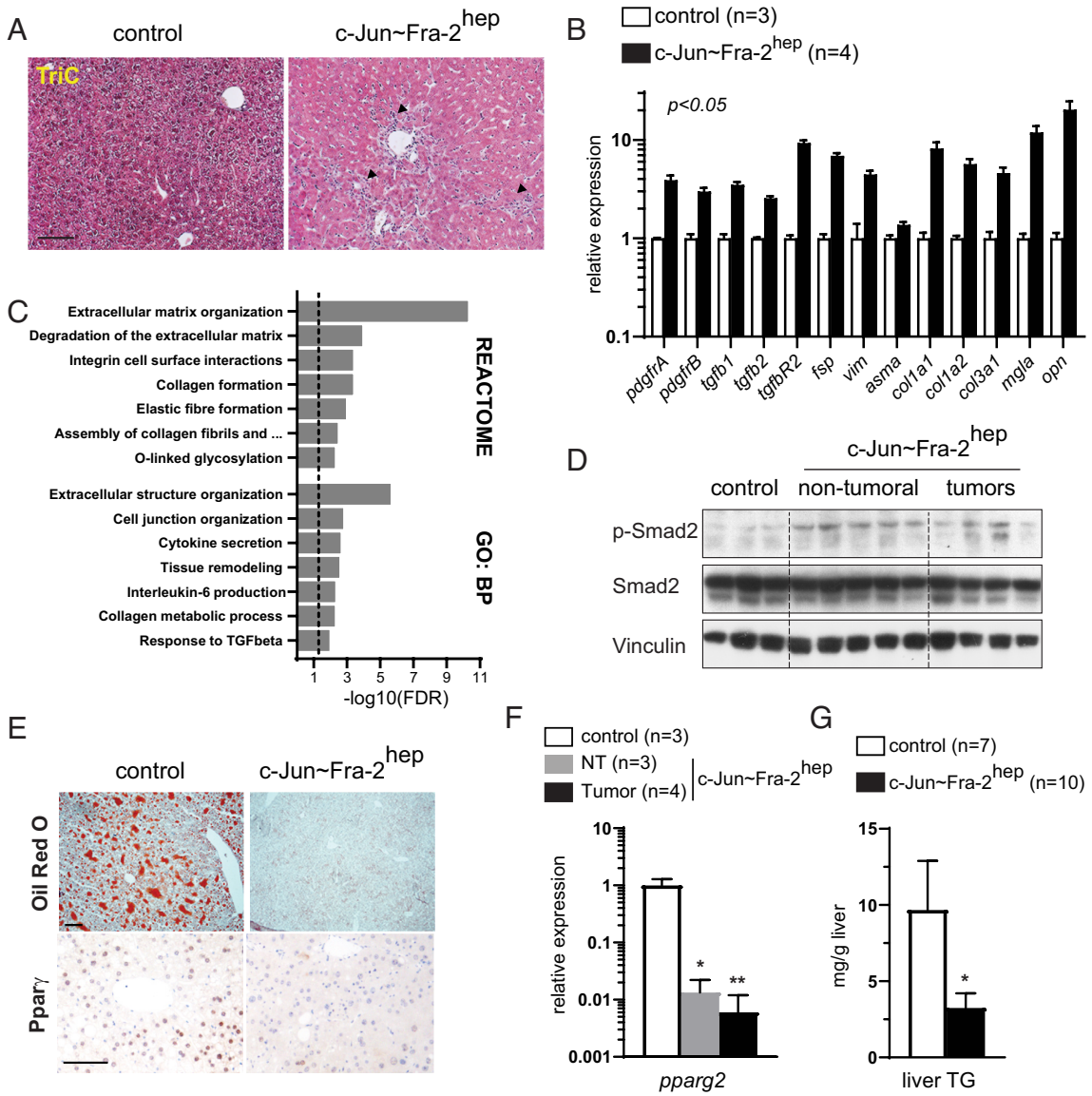

Fig. 3. Fibrosis and lipid metabolism in c-Jun~Fra-2^{hep} livers. (*A*) Masson Trichrome staining of c-Jun~Fra-2^{hep} and control liver sections at 2 mo. Bar = 100 µm, arrows point to fibrotic areas. (*B*) qRT-PCR quantification of fibrosis-associated genes in c-Jun~Fra-2^{hep} livers compared to controls at 2 mo, $P < 0.05$ for each mRNA. (*C*) Overrepresentation analysis (ORA, WebGestalt) of upregulated genes c-Jun~Fra-2^{hep} livers at 2 mo (RNAseq, n = 6 controls and 3 mutants) using Pathways/Reactome (enrichment > 2.6) and Gene Ontology/Biological processes (GO: BP, enrichment > 1.96) terms. The dotted line shows the adjusted FDR cut-off of <0.05. (*D*) Immunoblot for total and phosphorylated Smad2 in liver extracts from c-Jun~Fra-2^{hep} mice (NT and tumors) and controls. (*E*) Pparγ IHC and Oil Red O staining in c-Jun~Fra-2^{hep} (NT) and control livers at 9 mo. Bar = 100µm. (*F*) qRT-PCR quantification of *pparg2*, encoding Pparγ in c-Jun~Fra-2^{hep} tumors and NT liver areas compared to controls. (*G*) Liver triglycerides (TG) content in c-Jun~Fra-2^{hep} mice compared to controls at 9 mo. Vinculin is used to control immunoblot loading. Bars = means ± SEM, n ≥ 3. *$P < 0.05$, **$P < 0.01$, ***$P < 0.001$ (*t* test to controls).

c-Jun~Fra-2 Binds a *c-myc* 3′ Enhancer and Increases c-Myc and Myc Target Gene Expression. c-Myc is central to HCC pathogenesis and is connected to the IL6/JAK/Stat3 and PI3K/AKT/GSK3β pathways (43, 44). Consistent with the prominent enrichment in Myc-related murine and human liver cancer signatures (Fig. 2*B*) and the increased IL6/JAK/Stat3 and PI3K/AKT/GSK3β pathway activities (Fig. 2 *H* and *I* and *SI Appendix*, Fig. S2 *I–K*), c-Myc protein expression was increased in c-Jun~Fra-2^{hep} livers at 2 and 9 mo (Fig. 4*A* and *SI Appendix*, Fig. S4*A*). *c-myc* mRNA was also increased at 2 mo, but not in age-matched Jun~Fra-1^{hep} or Fra^{hep} mice (*SI Appendix*, Fig. S4*B*). *foxm1*, an HCC-relevant protein often connected to Myc (45), was also increased (*SI Appendix*, Fig. S4*C*), along with a panel of c-Myc target genes (Fig. 4*B*).

A 3′ enhancer, 1.4 kb downstream of the MYC transcriptional stop, is bound and activated by JUN-containing dimers in human colorectal cancer cells, cooperatively with β-catenin/TCF4 (46). This Wnt-responsive enhancer (WRE) is conserved in the mouse, including the AP-1 consensus motif TGACTCA, and a similar motif was identified in the *c-myc* promoter (Fig. 4*C*). Chromatin immunoprecipitation (ChIP) using hepatic chromatin from c-Jun~Fra-2^{hep} mice at 2 mo and Fra-2 (Fig. 4*D*) or Flag (Fig. 4 *E* and *F*) antibodies followed by quantitative PCR (ChIP-qPCR) revealed that c-Jun~Fra-2 efficiently bound the *c-myc*-WRE and the AP-1-responsive Dusp1 promoter used as a positive control, but not the c-myc promoter. The enrichment in WRE ChIP-qPCR fragments was negligible, when hepatic chromatin from Fra-2^{hep} mice was employed (Fig. 4*F*), consistent with unaltered *c-myc* expression in these samples (*SI Appendix*, Fig. S4*B*). Transient transfection experiments using the murine AML12 liver cell line revealed that c-Jun~Fra-2 expression increased endogenous *c-myc* mRNA along with the activity of a *c-myc*-WRE luciferase reporter, while Fra-2 had little to no effect (Fig. 4*G*).

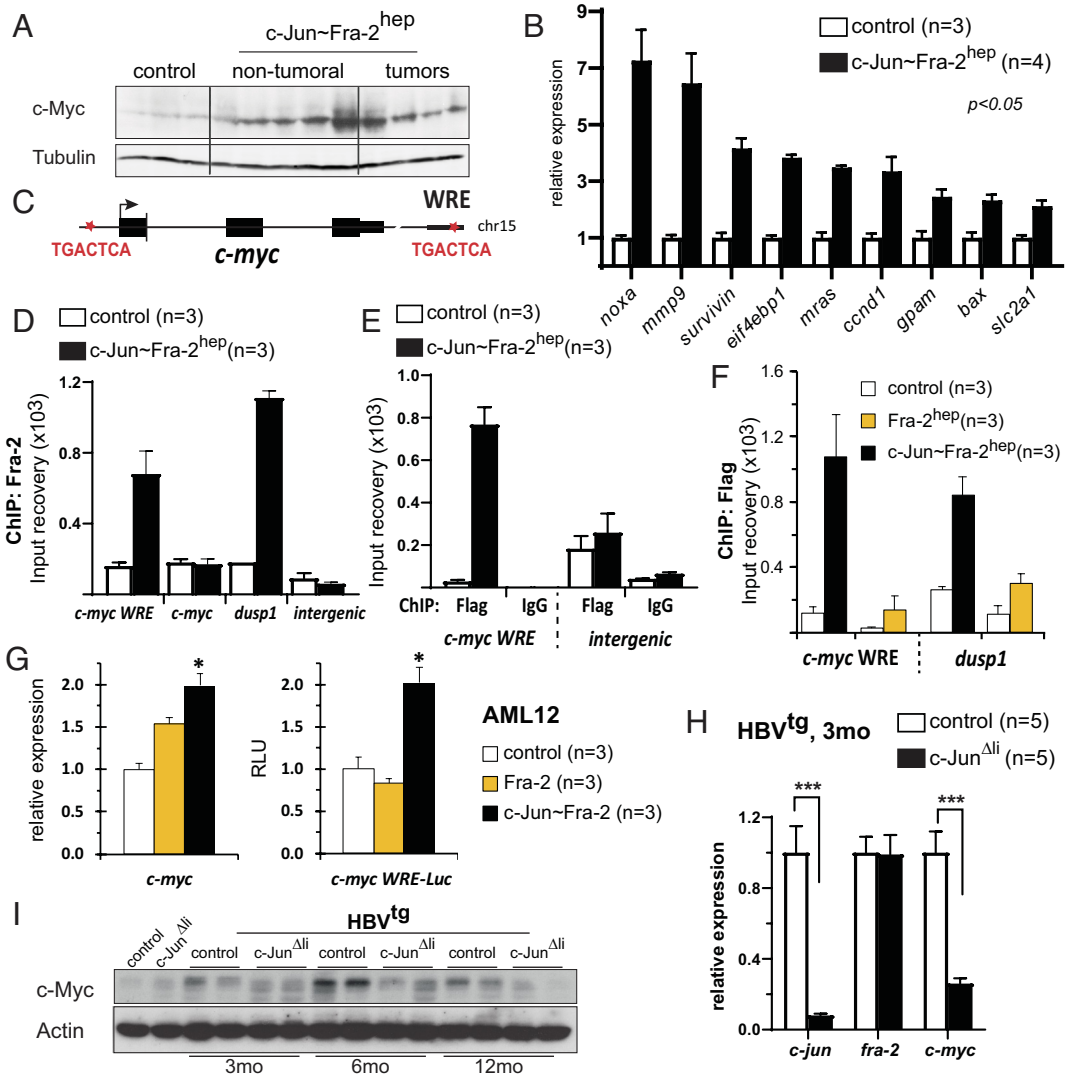

Fig. 4. Transcriptional control of c-Myc by c-Jun~Fra-2 in the liver. (*A*) Immunoblot analyses of c-Myc in liver extracts from c-Jun~Fra-2^{hep} mice (NT and tumors) and controls. (*B*) qRT-PCR quantification of c-Myc target genes c-Jun~Fra-2^{hep} livers at 2 mo, $P < 0.05$ for each mRNA. (*C*) Schematic of the murine *c-myc* gene indicating the putative AP-1 binding site elements (TGACTCA) in the promoter and the 3′ enhancer (WRE). (*D*) Fra-2 Chromatin immunoprecipitation (ChIP)-qPCR for the *c-Myc* 3′ enhancer (WRE) and promoter in livers from c-Jun~Fra-2^{hep} mutants and controls at 2 mo of transgene expression (off Dox at weaning). An AP-1 binding sequence from the *Dusp1* promoter and an intergenic area are included as positive and negative controls, respectively. (*E*) Flag and IgG Chromatin immunoprecipitation (ChIP)-qPCR for the *c-Myc* 3′ enhancer (WRE) and an intergenic area in livers from c-Jun~Fra-2^{hep} and Fra-2^{hep} mutants and controls at 2 mo. (*F*) Flag Chromatin immunoprecipitation (ChIP)-qPCR for the *c-Myc* 3′ enhancer (WRE) and *Dusp1* promoter in livers from c-Jun~Fra-2^{hep}, Fra-2^{hep} mutants and controls at 2 mo. (*G*) Functional validation in the murine AML12 liver cell line by transient transfection of Fra-2 or c-Jun~Fra-2 expression vectors, followed by *c-myc* qRT-PCR (*Left*) or luminescence measurement of a cotransfected c-Myc 3′ enhancer luciferase reporter (*Right*). (*H*) *c-jun*, *fra-2,* and c-*myc* qRT-PCR in livers from HBV transgenic mice (HBV^{tg}), lacking *c-jun* expression (c-Jun$^{\Delta li}$) in the liver compared to c-Jun-proficient HBV^{tg} littermates at 3 mo of age. (*I*) c-Myc immunoblot in liver extracts from c-Jun$^{\Delta li}$ HBV transgenic mice compared to HBV^{tg} c-Jun-proficient littermates over time. Two samples from mice not carrying the HBV transgene are included. Tubulin and Actin are used to control immunoblots loading. Bars = means ± SEM, n ≥ 3. *$P < 0.05$, **$P < 0.01$, ***$P < 0.001$.

c-myc expression was next evaluated in experimental HCC models with Fra-2 or c-Jun deficiency. Hepatic *c-myc* and *c-jun* expression was unchanged upon injection of the chemical carcinogen DEN to adult Fra-2$^{\Delta li}$ mice lacking Fra-2 in hepatocytes (*SI Appendix*, Fig. S4*D*). Furthermore, DEN-induced tumorigenesis was similar between Fra-2$^{\Delta li}$ and Fra-2-proficient littermates, as were serum AFP and ALT (*SI Appendix*, Fig. S4 *E* and *F*) and *c-myc* and *c-jun* expression in isolated tumors (*SI Appendix*, Fig. S4*G*). Mice lacking hepatic c-Jun are resistant to experimental HCC paradigms (13, 15, 17, 18) and a significant reduction in *c-myc* mRNA (Fig. 4*H*) and protein (Fig. 4*I*) expression are observed in c-Jun$^{\Delta li}$ livers during HBV-driven tumorigenesis (18). These data indicate that Fra-2 is dispensable, while c-Jun is needed to modulate c-myc expression, at least in the context of DEN- and HBV-induced tumorigenesis, respectively.

We next explored the connection between JUN, FRA2, and MYC in human liver cancer. Datamining of genome-wide Chromatin immunoprecipitation-Sequencing (ChIPseq) of HepG2 hepatoma cells (47) revealed JUN- and FRA2- ChIPseq peaks in a transcriptionally active genomic area consistent with the MYC WRE (*SI Appendix*, Fig. S4*H*). Furthermore, *MYC* mRNA expression was abrogated in HepG2 cells upon CRISPR/cas9 deletion of the MYC WRE, while it was increased after transient expression of c-Jun~Fra-2 in the parental cell line (*SI Appendix*, Fig. S4*I*) and decreased upon siRNA knock-down of JUN or JUNB (*SI Appendix*, Fig. S4*J*). HCC RNAseq data from treatment-naïve patients (TCGA-LIHC) generated by The Cancer Genome Atlas (48) were next explored. MYC expression, reported as the average number of "Fragments Per Kilobase of exon per Million reads" (FPKM), correlated with each of JUN and FRA2 independently (*SI Appendix*, Fig. S4*K*). Cohorts with high (HH) or low (LL) JUN and FRA2 expression were next defined, corresponding to 37% and 27% of the samples, respectively (*SI Appendix*, Fig. S4 *K*, *Right*). Strikingly, MYC, FOXM1, and Cyclin D1 (CCND1) expression was found higher (*SI Appendix*, Fig. S4*L*) and overall survival lower (*SI Appendix*, Fig. S4*M*) in the HH group. Taken together these data indicate that the modulation of *c-myc* expression by c-Jun/Fra-2 is likely also occurring in human hepatocytes and could be relevant to HCC progression.

c-Jun~Fra2^{hep} Tumors Are Reversible, But Addicted to *c-myc* Expression. We next investigated whether c-Jun~Fra-2 is necessary to maintain the tumor phenotype by utilizing the "tetracycline switch" in c-Jun~Fra-2^{hep} mice. c-Jun~Fra-2 was induced for 9 mo, and the mice subsequently put back on Dox to halt c-Jun~Fra-2 expression and killed 6 mo later (Fig. 5*A*). At this OFF endpoint, approximately 2/3 of the c-Jun~Fra-2^{hep} mice, hereafter termed "reverted", had no visible liver nodule at necropsy, while the rest of the c-Jun~Fra-2^{hep} mice, hereafter "escapers", presented at least one visible surface nodule (Fig. 5*B*). Liver to body weight ratio (*SI Appendix*, Fig. S5*A*) and serum AFP (Fig. 5*C*) were comparable to controls in the reverted mice, while half (liver/body) to most (AFP) escapers had higher values and were similar to c-Jun~Fra-2^{hep} mice killed after 9 mo of c-Jun~Fra-2 expression (ON). Serum ALT at end point was more heterogeneous, but escapers were still in the higher ranges (*SI Appendix*, Fig. S5*A*).

Six c-Jun~Fra-2^{hep} mice, hereafter termed mutant-1 to -6, were next followed longitudinally by liver ultrasonography (US) and serum monitoring along the reversion protocol. These mice had 1 to 3 tumors of variable size and roughly similar AFP, ALT, and ALP values (*SI Appendix*, Table S1*A*). While all 6 c-Jun~Fra-2^{hep} mice displayed a sharp drop in serum AFP, approaching control levels after 8 wk, AFP increased again in mutant-5 and even more in mutant-6 (*SI Appendix*, Fig. S5*B*). High ALT concentrations were also measured at end point in these 2 mice, whereas ALP was comparable to control values in all 6 c-Jun~Fra-2^{hep} mice (*SI Appendix*, Table S1*A*). US monitoring revealed that the fate of the individual tumors was heterogeneous and rather independent of their initial size or mouse of origin (Fig. 5*D* and *SI Appendix*, Table S1*A*). Some tumors regressed to very small (T3 in mutant-4 and T1 in mutant-6) or below detection limit (T1 and T2 in mutant-4, all tumors in mutant-1 and mutant -2), while other tumors initially regressed, but resumed growing after a variable period (T1 in mutant-5 and T2 in mutant-6). We also observed the emergence of new tumors, with different sizes, latencies, and growth kinetics, such as T3* in mutants 5 and 6 (Fig. 5*D* and *SI Appendix*, Table S1*A*). Although we cannot rule out that these tumors were overlooked at start due to US limitations, it remains striking that the timing of the AFP "rebound" in mutants 5 and 6 roughly corresponds to the regrowth of preexisting tumors and/or detection of new tumors in these mice (Fig. 5*D* and *SI Appendix*, Fig. S5*B*).

Liver tumors were next dissected from a group of escapers, together with NT areas and compared to (tumor-free) livers from reverted and control littermates, as well as NT and tumoral areas from mice killed after 9 mo of c-Jun~Fra-2 expression (ON). qRT-PCR for *fra-2* (Fig. 5*E*) and *c-Jun~Fra-2* (*SI Appendix*, Fig. S5*C*) confirmed that c-Jun~Fra-2 was barely detectable in the samples collected at the OFF endpoint. However, while *c-myc* mRNA was decreased to control levels in reverted livers and in escapers' NT areas, escaping tumors had high *c-myc* expression (Fig. 5*F*) and detectable c-Myc-positive cells by IHC (*SI Appendix*, Fig. S5*D*). qRT-PCR analyses revealed high expression of oncofetal, cancer cell stemness, HCC, and replicative senescence markers in escaping tumors (Fig. 5*G*), as well as *foxm1*, *p21,* and a panel of c-Myc target genes (*SI Appendix*, Fig. S5*E*), while the corresponding NT areas displayed an expression profile more similar to controls (Fig. 5*G* and *SI Appendix*, Fig. S5*E*). These data are consistent with c-Myc being an essential molecular determinant of tumor formation and maintenance in c-Jun~Fra-2^{hep} mice. Interestingly, some of the escaping tumors displayed increased Fos mRNA (*SI Appendix*, Fig. S5*F*) and protein (*SI Appendix*, Fig. S5*D*). As *c-myc* and c-Myc target gene expression is increased in the preneoplastic livers of Fos^{hep} mice (*SI Appendix*, Fig. S5*G*), Fos-containing AP-1 dimers likely substitute for c-Jun~Fra-2 to maintain *c-myc* expression, at least in a subset of escaping tumors.

Therapeutic Value of a Bromodomain and Extra-Terminal motif Inhibitor (BETi) in c-Jun~Fra-2^{hep} Mice. The therapeutic potential of interfering pharmacologically with c-Myc expression and activity was tested in c-Jun~Fra-2^{hep} mice employing JQ-1, a Bromodomain and Extra-Terminal motif inhibitor (BETi) widely used in basic research (49, 50). When c-Jun~Fra-2 was induced for 2 mo prior to 4 wk of treatment (*SI Appendix*, Fig. S6*A*), JQ-1 decreased hepatic c-Myc protein expression (Fig. 6*A*), while c-Jun~Fra-2 was not affected (Fig. 6*A* and *SI Appendix*, Fig. S6*B*). Hepatic *c-myc* mRNA was unchanged, when comparing JQ-1- to vehicle-treated c-Jun~Fra-2^{hep} mice, while mRNA expression of *foxm1*, *ccna2,* and a panel of c-Myc target genes was decreased (*SI Appendix*, Fig. S6*C*). Serum AFP, ALT, and AST were ameliorated in JQ-1-treated c-Jun~Fra-2^{hep} mice, while ALP remained high (*SI Appendix*, Fig. S6 *D* and *E*). Finally, Ki67, Cyclin D1, and γH2AX indexes were reduced upon JQ1 treatment (*SI Appendix*, Fig. S6*F*), consistent with a potential beneficial effect of JQ1 on the preneoplastic events occurring in c-Jun~Fra-2^{hep} mice.

Next, 6 c-Jun~Fra-2^{hep} mice were randomized at 9 mo into 2 treatment groups and followed during 8 wk to assess the effect of JQ1 on already established tumors (*SI Appendix*, Fig. S6*A*). At end

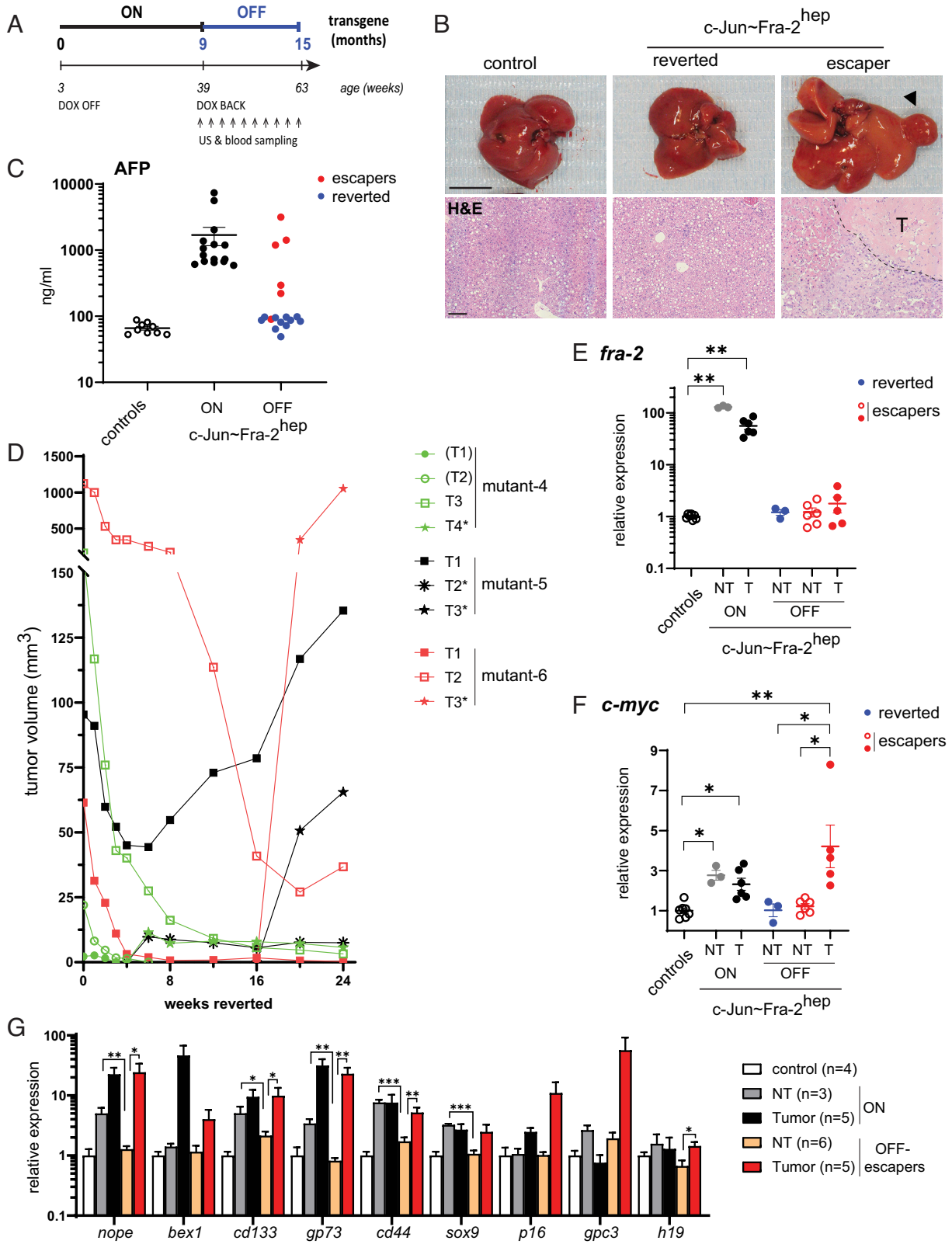

Fig. 5. Reversibility and oncogene addiction(s) of c-Jun~Fra-2^{hep} liver tumors. (*A*) Experimental design and timeline of the reversion experiment: c-Jun~Fra-2^{hep} mutants with 9 mo of transgene expression (off Dox at weaning) were put back on Dox, followed over time and compared to littermate controls and to unreverted mice (killed at 9 mo). US: ultrasonography. (*B*) Liver morphology and histology in c-Jun~Fra-2^{hep} reverted and escaper mutants compared to control. Bar = 1 cm (*Top*) and 100 μm (H&E: Hematoxylin and Eosin, *Bottom*), tumors (T) are indicated by arrows and dotted line. (*C*) Serum AFP at end point in individual mice, reversion escapers are marked in red, controls values were comparable between the ON and OFF time points and plotted together. (*D*) Tumor monitoring by ultrasonography. Individual tumor volume from 3 reverted mice showing reversion escapers plotted over time; neotumors are indicated with an asterisk and regressed tumors between parentheses. *fra-2* (*E*) and *c-myc* (*F*) qRT-PCR in tumors (T) and NT liver areas from nonreverted (ON) and reverted (OFF, 24 wk) c-Jun~Fra-2^{hep} mice compared to controls. Reversion escapers are plotted separately (red), controls values were comparable between the ON and OFF time points and plotted together. (*G*) qRT-PCR quantification of oncofetal, stemness, and senescence-associated genes in tumors and NT liver areas from c-Jun~Fra-2^{hep} mice either nonreverted (ON) or with tumors that escaped reversion (OFF, 24 wk) compared to (pooled) controls. In the dot plots, means ± SEM are included. Bars = means ± SEM. *P < 0.05, **P < 0.01, ***P < 0.001 (*t* test).

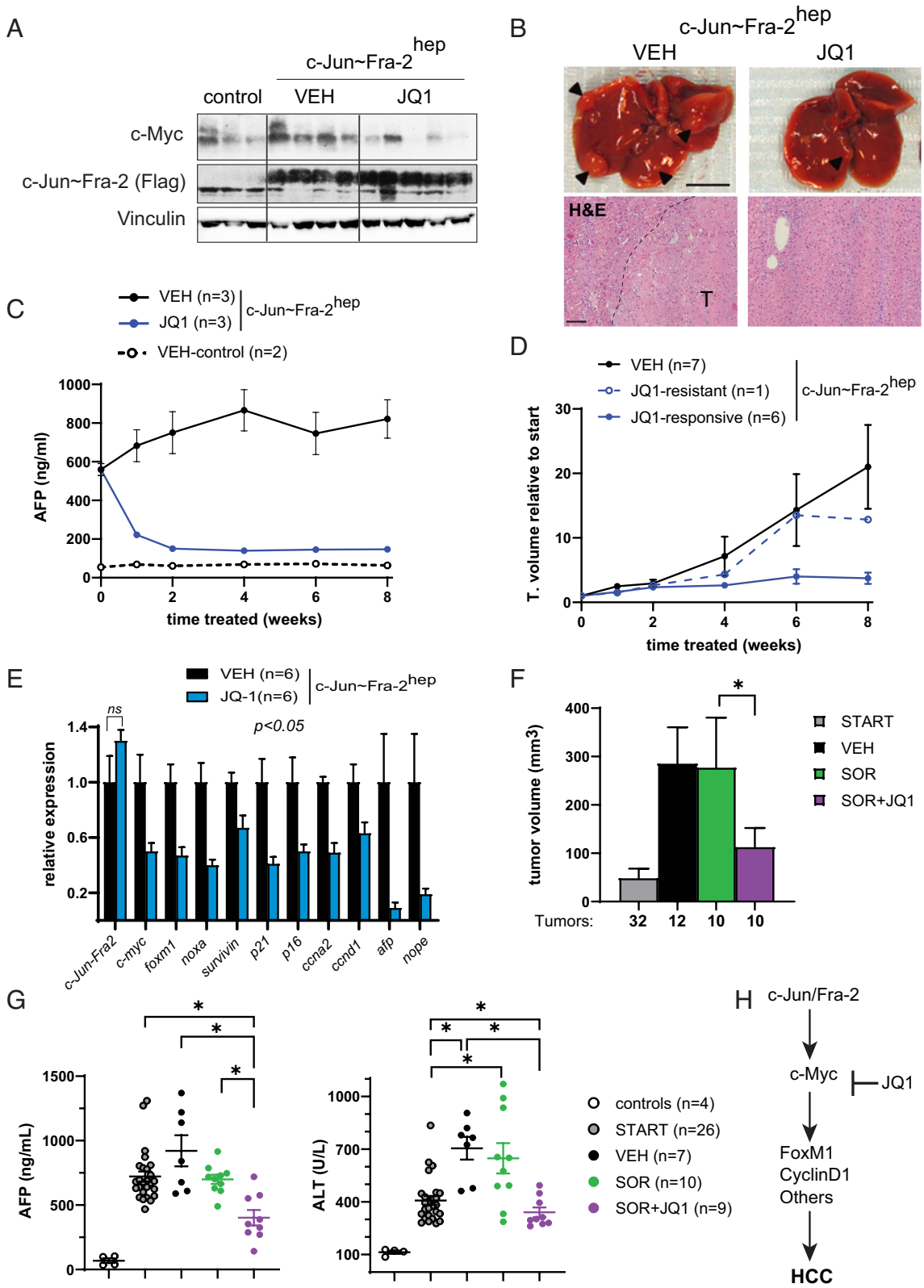

Fig. 6. Therapeutic interventions in c-Jun~Fra-2^{hep} mutant mice. (*A*) c-Myc and Flag immunoblot in liver extracts of c-Jun~Fra-2^{hep} mice treated 2 mo after transgene induction with JQ1 or vehicle (VEH) during 4 wk. Vinculin is used to control loading. (*B–E*) c-Jun~Fra-2^{hep} mutants with 9 mo of transgene expression (off Dox at weaning) were randomized and treated with JQ1 or VEH, during 2 mo. (*B*) Liver morphology at endpoint. Bar = 1 cm (*Top*) and 100 μm (H&E: Hematoxylin and Eosin, *Bottom*), tumors (T) are indicated by arrows and dotted line. (*C*) Serum AFP over time. (*D*) Tumor monitoring by US: The average tumor volume from 3 VEH or JQ1-treated mice is plotted relative to start (randomization), with the JQ1-resistant tumor plotted separately (dotted line). (*E*) qRT-PCR quantification of c-Jun~Fra-2, *c-myc*, c-Myc targets and cancer-relevant genes at endpoint in liver samples comparing VEH- and JQ1-treated (responsive) c-Jun~Fra-2^{hep} mice, $P < 0.05$ for each mRNA except *c-Jun~Fra-2*. (*F* and *G*) c-Jun~Fra-2^{hep} mutants with 9 mo of transgene expression (off Dox at weaning) were randomized for VEH, Sorafenib (SOR), or SOR+JQ1 during 2 mo. (*F*) US quantification of tumor volume at start and endpoint. The indicated number of analyzed tumors corresponds to the four groups of tumor-bearing mice analyzed in *G*. (*G*) Serum AFP (*Left*) and ALT (*Right*) at start and endpoint. 4 VEH-treated control mice are included as healthy reference. Bars = means ± SEM. In dot plots and graphs, means ± SEM are plotted. *$P < 0.05$ (*t* test). (*H*) Working model how c-Jun/Fra-2 dimers promote liver cancer through modulating c-Myc expression.

point necropsy, most JQ-1-treated c-Jun~Fra-2^{hep} mice had smaller and fewer liver nodules compared to their vehicle-treated counterparts (Fig. 6*B*). Serum AFP rapidly decreased in treated c-Jun~Fra-2^{hep} mice and remained stable until end point, although slightly higher than controls (Fig. 6*C* and *SI Appendix*, Table S1*B*). ALT and AST were still high at end point in JQ1-treated c-Jun~Fra-2^{hep} mice, but unlike vehicle-treated counterparts, liver transaminases did not increase over time (*SI Appendix*, Fig. S6*G*). In contrast, ALP slightly decreased, but remained comparable between treatment arms (*SI Appendix*, Fig. S6*G*). Ultrasound follow-up revealed that JQ-1 had a tumor-static effect: While tumors in vehicle-treated c-Jun~Fra-2^{hep} mice increased in size over time, 6 out of 7 tumors in JQ-1-treated mice remained relatively stable and no new tumors were detected (Fig. 6*D* and *SI Appendix*, Table S1*B*). qRT-PCR analyses comparing JQ-1-responsive to vehicle-treated tumors revealed decreased expression of *c-myc,* along with *foxm1* and other cell cycle- HCC-, immune- and fibrosis-related transcripts, while *c-Jun~Fra-2* was not affected (Fig. 6*E* and *SI Appendix*, Fig. S6*H*). Furthermore, we combined JQ1 with Sorafenib, a receptor tyrosine kinase inhibitor widely used to treat HCC. Sorafenib alone had no noticeable effect on tumor size after 8 wk of treatment (Fig. 6*F*), consistent with reports indicating Sorafenib resistance in HCC with high JUN/JNK (51, 52). JQ1 also slowed liver tumor growth in c-Jun~Fra-2^{hep} mice treated with when coadministered with Sorafenib (Fig. 6*F*) and reduced circulating AFP and ALT at endpoint (Fig. 6*G*). Taken together, these results indicate that BETi should be considered for HCC therapy, particularly in patients with high AP-1/Myc expression.

Discussion

While GEMMs are essential for advancing the cellular and molecular understanding of liver cancer (17), the combinatorial character of AP-1 homo- and heterodimers complicates the identification of dimer-specific functions, when using conventional monomer-based gain- or loss-of-function GEMMs. Using a single-chain, forced dimer strategy approach, the present study dissects the contribution of a specific c-Jun/Fra-2 AP-1 dimer to HCC pathogenesis in vivo. Hepatic expression of c-Jun~Fra-2 leads to hepatocyte proliferation, decreased hepatic fat content, moderate liver inflammation, and limited fibrosis, with the subsequent development of liver tumors that have HCC characteristics. We identify a crucial pathogenic interaction between c-Jun/Fra-2 and c-Myc (Fig. 6*H*) as an important initiating event and identify the consequences of switching off the c-Jun~Fra-2 oncogenic driver or therapeutically targeting c-Myc activation in established liver tumors.

Mice expressing Fra-1, Fra-2, or c-Jun~Fra-2 in the liver express lower levels of Pparγ and are protected from steatohepatitis (22, 24). Repression of Pparγ is maintained during liver carcinogenesis in c-Jun~Fra-2^{hep} mice, while a c-Jun~Fra-1 dimer has apparently no effect. As Pparγ expression across Fra-1/2^{hep} and c-Jun~Fra-1/2^{hep} mice is not correlated with the occurrence of liver tumors, decreased hepatic Pparγ is likely not causally involved in the early c-Jun~Fra-2-driven oncogenic events. However, it might potentiate transformation, as Pparγ$^{+/-}$ mice are more susceptible to DEN-induced HCC (53). Strikingly, signs of mild inflammation, fibrosis, and even ER stress, are observed in c-Jun~Fra-2^{hep} livers despite a dyslipidemic, low hepatic fat context. Future experiments will clarify whether any or all of these events are essential for tumorigenesis and how they occur independently of steatosis. The c-Jun~Fra-2^{hep} GEMM constitutes a convenient model to dissect the interactions between preneoplastic or fully transformed hepatocytes and their nonparenchymal environment.

c-Myc and Myc pathway activation is a major oncogenic event in many tumor types including HCC (54, 55). A modest but consistent increase in c-Myc mRNA and protein expression was measured in livers of c-Jun~Fra-2^{hep} mice already before tumors were observed. Importantly, and consistent with a crucial role for increased c-Myc in c-Jun~Fra-2–driven hepatocyte transformation, tumors that escaped switching off c-Jun~Fra-2 maintained c-Myc expression, while it was decreased to control levels in the adjacent NT areas. In addition, the tumor-static effect of JQ-1, which decreased Myc expression and activity in c-Jun~Fra-2 tumors, is in line with the idea that these tumors are addicted to increased c-Myc expression that is initiated by the c-Jun/Fra-2 AP-1 dimer.

Several signaling pathways, such as IL6/JAK/Stat3 and PI3K/AKT/GSK3β (43, 44), both elevated in c-Jun~Fra-2^{hep} livers and tumors, can increase c-Myc expression. These pathways might also contribute to maintain c-Myc expression in tumors escaping switching off c-Jun~Fra-2, together or along with increased Fos expression that is observed in some escaping tumors. Using Jun~Fra-2^{hep} mice, mouse, and human liver cell lines and publicly available human cell lines and human liver cancer datasets, we demonstrate that c-Jun/Fra-2 activates *c-myc* transcription by binding a conserved 3′ enhancer in the *c-myc* gene. Importantly, hepatocyte-specific expression of the closely related c-Jun~Fra-1 dimer, or freely dimerizing Fra-1 or Fra-2 monomers, had no impact on *c-myc* expression and did not lead to spontaneous tumors. Conversely, preneoplastic livers expressing Fos (19) had elevated *c-myc* mRNA, while increased *fos* mRNA was observed in three out of five tumor escapers that maintained c-Myc expression. These data indicate that only specific AP-1 complexes, such as c-Jun/Fra-2 and Fos-containing dimers can activate *c-myc* transcription in hepatocytes. Ongoing work using a similar forced dimer strategy will certainly shed light on the identity of the Fos-containing dimers modulating *c-myc* in hepatocytes. A likely consequence of this functional dimer redundancy, supported by loss-of-function experiments, is that no Jun or Fos protein is essential for *c-myc* expression. In HepG2 cells, where Chromatin immunoprecipitation (ChIP) experiments indicate that c-Jun and Fra-2 form a functional dimer on the *MYC*3' enhancer, knock-down of either JUN or JUNB moderately decreased *MYC* mRNA, while a significant reduction in *c-myc* mRNA and protein was observed during HBV-driven carcinogenesis in mice lacking hepatic c-Jun. However, c-Myc protein expression was unaltered in DEN-induced c-Jun$^{\Delta li}$ liver tumors, while hepatic c-Myc decreased upon genetic inactivation of the AP-1-upstream kinase JNK1 (14). Bulk RNAseq analyses of Fos-expressing and Fos-deficient livers (19) indicated that hepatic *c-myc* expression was increased in c-Fos^{hep}, but unchanged in DEN-treated c-Fos$^{\Delta li}$ mice. c-Myc transcription is also not affected by the single inactivation of Fra-2 in hepatocytes and Fra-2$^{\Delta li}$ mice, subjected here to an HCC paradigm, display unaltered DEN-induced tumorigenesis. While the consequences of inactivating other AP-1 monomers, such as JunB, JunD, and Fra-1 on hepatic *c-myc* expression and tumorigenesis remain to be formally tested, these experiments indicate that the requirement for AP-1-forming proteins to modulate *c-myc* expression during liver carcinogenesis is dimer- but also context- specific. Targeting one or multiple AP-1 dimers might not be a straightforward therapeutic option, although our in silico analysis of the TCGA-LIHC dataset, as well as preliminary immunehistochemical analyses of a set of HCC tumors, indicates that patient stratification according to JUN/FRA2 and MYC expression might help identifying patients likely to respond to such AP-1 and/or Myc-targeted therapies.

Despite being heterogeneous in size, molecular profiles, and growth kinetics, liver tumors arising in Jun~Fra-2^{hep} mice regressed upon switching off c-Jun~Fra-2 expression. However, a fraction of tumors relapsed and new tumors arose within few weeks, possibly in a c-Myc-dependent manner as indicated by the analyses of tumors collected 6 mo later. The cellular and molecular events occurring immediately after turning OFF c-Jun~Fra-2, the involvement of Fos-containing dimers, and their connection to the various protumorigenic functions of c-Myc certainly warrant further evaluation. Unbiased, possibly single-cell, RNA, and proteome profiling of a large number of tumors in different ON and OFF settings and subsequent comparison with the OMIC data generated using c-Myc-switchable liver mice (56, 57) will help narrowing down the essential molecular and cellular players.

Several therapeutic strategies targeting Myc, mostly indirectly, have been evaluated (58, 59). The early tool compound JQ-1 (49) and other Bromodomain and Extra-Terminal motif-family inhibitors (BETi) have preclinical benefits in several cancers, often through Myc/Myc target suppression (60). While a Myc-independent antitumorigenic decrease in Fra-1 transcription has been reported after BETi (61), JQ-1 does not impact c-Jun~Fra-2 mRNA or protein expression and its positive effects in c-Jun~Fra-2 ^{hep} tumors appears to be Myc-dependent. This is also in line with the idea that Myc-dependent tumorigenesis is reversible even when Myc is not the initiating oncogenic lesion, as shown in lung adenocarcinoma induced by oncogenic Ras (62), an upstream activator of AP-1.

Despite a wealth of studies, there is no effective therapy for HCC due to limited mechanistic knowledge of this heterogeneous disease and the lack of biomarkers to select clinical trial patients most likely to benefit from a specific therapy. HCC prevention by limiting viral hepatitis, currently accounting for 75% of liver cancer deaths, remains the key strategy, while Sorafenib is still a standard of care for HCC in low income countries, despite limited efficacy. The increased relevance of nonviral risk factors is a major concern aggravated by the poor prognosis of HCC patients, even in high income countries with the widest portfolio of therapeutic options and where immunotherapies have become first-line treatment for advanced HCC. While BETi have shown mixed results as single agents (50, 60), immunotherapies are costly and have yet to fulfill their promises (2, 3). Combination therapies involving BETi, for example, flight tested in this preclinical model, may enhance treatment effectiveness for selected patients with high AP-1/Myc expression and might help achieve widespread access to affordable and more efficient HCC treatment.

Materials and Methods

Detailed methods are provided in *SI Appendix*. Briefly, adult male Jun~Fra-2^{hep} mice were killed at different time point of transgene induction (typically 2 mo and 9 mo) and the livers harvested for histological, molecular, and biochemical analyses. Blood collected by submandibular vein or cardiac puncture was used for longitudinal monitoring. Murine AML12 and human HepG2 liver-derived cell lines were used for in vitro experiments.

Data, Materials, and Software Availability. RNAseq datasets are deposited as series GSE261005 in the Gene expression omnibus (GEO) archive(30). Noncommercially available materials and reagents are available upon reasonable request. All other data are included in the article and/or *SI Appendix*.

ACKNOWLEDGMENTS. We thank Guillermo Medrano for help with mouse procedures and Vanessa Bermeo for assisting with tissue sections and staining. Birgit Hockenjos for analyzing Jun$^{\Delta li}$, HBV^{Tg} liver samples, Stefanie Stolzlechner for IHC troubleshooting, and Sophia Derdak from the Core Facilities of the Medical University of Vienna, a member of the Vienna Life-Science Instruments initiative, for analysis of bulk RNA-seq data. We are grateful to the Molecular Imaging, Mouse Genome Editing, Histopathology and Genomics Core Units of the Spanish National Cancer Research Centre for efficient service. We are very grateful to Drs. Douglas Hanahan, Kazuhiko Matsuoka, Robert Eferl, Nabil Djouder, Esteban Gurzov, and Emilio Casanova and to the members of the Wagner laboratory for comments and discussions. The Wagner laboratory is supported by the ERC (AdG 2016-741888-CSI-Fun), a H2020 – MSCA grant (ITN 2019-859860-CANCERPREV) and the Medical University of Vienna.

Author affiliations: [a]Laboratory Genes and Disease, Department of Laboratory Medicine, Medical University of Vienna, 1090, Vienna, Austria; [b]Genes, Development and Disease Group, National Cancer Research Centre, 28029, Madrid, Spain; [c]Department of Biomedicine, University of Aarhus, 8000, Aarhus, Denmark; [d]Department of Medicine II, University Hospital and Faculty of Medicine, 79106, Freiburg, Germany; and [e]Laboratory Genes and Disease, Department of Dermatology, Medical University of Vienna, 1090, Vienna, Austria

Author contributions: L.B. and S.C.H. designed research; L.B., S.C.H., A.G.-C., M.K.T., and P.H. performed research; L.B. analyzed data; A.G.-C. provided essential technical assistance; E.F.W. directed the study, approved the data; and L.B. and E.F.W. wrote the paper.

1. H. Sung *et al.*, Global cancer statistics 2020: GLOBOCAN estimates of incidence and mortality worldwide for 36 cancers in 185 countries. *CA Cancer J. Clin.* **71**, 209–249 (2021).
2. A. Alqahtani *et al.*, Hepatocellular carcinoma: Molecular mechanisms and targeted therapies. *Medicina (Kaunas)* **55**, 526 (2019).
3. J. Hou, H. Zhang, B. Sun, M. Karin, The immunobiology of hepatocellular carcinoma in humans and mice: Basic concepts and therapeutic implications. *J. Hepatol.* **72**, 167–182 (2020).
4. C. Campani, J. Zucman-Rossi, J. C. Nault, Genetics of hepatocellular carcinoma: From tumor to circulating DNA. *Cancers (Basel)* **15**, 817 (2023).
5. G. He, M. Karin, NF-kappaB and STAT3 - key players in liver inflammation and cancer. *Cell Res.* **21**, 159–168 (2011).
6. E. F. Wagner, A. R. Nebreda, Signal integration by JNK and p38 MAPK pathways in cancer development. *Nat. Rev. Cancer* **9**, 537–549 (2009).
7. R. Eferl, E. F. Wagner, AP-1: A double-edged sword in tumorigenesis. *Nat. Rev. Cancer* **3**, 859–868 (2003).
8. G. L. Rampioni Vinciguerra *et al.*, Role of Fra-2 in cancer. *Cell Death Differ.* **31**, 136–149 (2023), 10.1038/s41418-023-01248-4.
9. E. Stepniak *et al.*, c-Jun/AP-1 controls liver regeneration by repressing p53/p21 and p38 MAPK activity. *Genes Dev.* **20**, 2306–2314 (2006).
10. I. Schulien *et al.*, The transcription factor c-Jun/AP-1 promotes liver fibrosis during non-alcoholic steatohepatitis by regulating Osteopontin expression. *Cell Death Differ.* **26**, 1688–1699 (2019).
11. P. Hasselblatt, M. Rath, V. Komnenovic, K. Zatloukal, E. F. Wagner, Hepatocyte survival in acute hepatitis is due to c-Jun/AP-1-dependent expression of inducible nitric oxide synthase. *Proc. Natl. Acad. Sci. U.S.A.* **104**, 17105–17110 (2007).
12. M. Fuest *et al.*, The transcription factor c-Jun protects against sustained hepatic endoplasmic reticulum stress thereby promoting hepatocyte survival. *Hepatology* **55**, 408–418 (2012).
13. R. Eferl *et al.*, Liver tumor development. c-Jun antagonizes the proapoptotic activity of p53. *Cell* **112**, 181–192 (2003).
14. L. Hui, K. Zatloukal, H. Scheuch, E. Stepniak, E. F. Wagner, Proliferation of human HCC cells and chemically induced mouse liver cancers requires JNK1-dependent p21 downregulation. *J. Clin. Invest.* **118**, 3943–3953 (2008).
15. K. Machida *et al.*, c-Jun mediates hepatitis C virus hepatocarcinogenesis through signal transducer and activator of transcription 3 and nitric oxide-dependent impairment of oxidative DNA repair. *Hepatology* **52**, 480–492 (2010).
16. L. Min *et al.*, Liver cancer initiation is controlled by AP-1 through SIRT6-dependent inhibition of survivin. *Nat. Cell Biol.* **14**, 1203–1211 (2012).
17. L. Bakiri, E. F. Wagner, Mouse models for liver cancer. *Mol. Oncol.* **7**, 206–223 (2013).
18. C. Trierweiler *et al.*, The transcription factor c-JUN/AP-1 promotes HBV-related liver tumorigenesis in mice. *Cell Death Differ.* **23**, 576–582 (2016).
19. L. Bakiri *et al.*, Liver carcinogenesis by FOS-dependent inflammation and cholesterol dysregulation. *J. Exp. Med.* **214**, 1387–1409 (2017).
20. M. K. Thomsen *et al.*, JUNB/AP-1 controls IFN-gamma during inflammatory liver disease. *J. Clin. Invest.* **123**, 5258–5268 (2013).
21. D. E. Smart *et al.*, JunD is a profibrogenic transcription factor regulated by Jun N-terminal kinase-independent phosphorylation. *Hepatology* **44**, 1432–1440 (2006).
22. S. C. Hasenfuss *et al.*, Regulation of steatohepatitis and PPARgamma signaling by distinct AP-1 dimers. *Cell Metab.* **19**, 84–95 (2014).
23. S. C. Hasenfuss, L. Bakiri, M. K. Thomsen, R. Hamacher, E. F. Wagner, Activator protein 1 transcription factor Fos-related antigen 1 (Fra-1) is dispensable for murine liver fibrosis, but modulates xenobiotic metabolism. *Hepatology* **59**, 261–273 (2014).
24. L. Bakiri, S. C. Hasenfuss, E. F. Wagner, A FATal AP-1 dimer switch in hepatosteatosis. *Cell Cycle* **13**, 1218–1219 (2014).
25. L. Bakiri, K. Matsuo, M. Wisniewska, E. F. Wagner, M. Yaniv, Promoter specificity and biological activity of tethered AP-1 dimers. *Mol. Cell Biol.* **22**, 4952–4964 (2002).

26. A. Kobeissy *et al.*, Protein induced by vitamin K absence or antagonist-II versus alpha-fetoprotein in the diagnosis of hepatocellular carcinoma: A systematic review with meta-analysis. *J. Clin. Med. Res.* **15**, 343–359 (2023).
27. X. Zhou *et al.*, MCM2 promotes the stemness and sorafenib resistance of hepatocellular carcinoma cells via hippo signaling. *Cell Death Discov.* **8**, 418 (2022).
28. M. Wang *et al.*, SOX9 enhances sorafenib resistance through upregulating ABCG2 expression in hepatocellular carcinoma. *Biomed. Pharmacother.* **129**, 110315 (2020).
29. M. B. Ruzinova *et al.*, SOX9 expression is superior to other stem cell markers K19 and EpCAM in predicting prognosis in hepatocellular carcinoma. *Am. J. Surg. Pathol.* **47**, 1–11 (2023).
30. L. Bakiri. Liver cancer development driven by the AP-1/c-Jun~Fra2 dimer through c-Myc. NCBI Gene Expression Omnibus. https://www.ncbi.nlm.nih.gov/geo/query/acc.cgi?acc=GSE261005. Deposited Mar 06, 2024.
31. A. Subramanian *et al.*, Gene set enrichment analysis: A knowledge-based approach for interpreting genome-wide expression profiles. *Proc. Natl. Acad. Sci. U.S.A.* **102**, 15545–15550 (2005).
32. A. M. Newman *et al.*, Determining cell type abundance and expression from bulk tissues with digital cytometry. *Nat. Biotechnol.* **37**, 773–782 (2019).
33. R. Carlessi *et al.*, Single-nucleus RNA sequencing of pre-malignant liver reveals disease-associated hepatocyte state with HCC prognostic potential. *Cell Genom.* **3**, 100301 (2023).
34. Y. Hoshida *et al.*, Integrative transcriptome analysis reveals common molecular subclasses of human hepatocellular carcinoma. *Cancer Res.* **69**, 7385–7392 (2009).
35. S. Boyault *et al.*, Transcriptome classification of HCC is related to gene alterations and to new therapeutic targets. *Hepatology* **45**, 42–52 (2007).
36. H. G. Woo *et al.*, Identification of a cholangiocarcinoma-like gene expression trait in hepatocellular carcinoma. *Cancer Res.* **70**, 3034–3041 (2010).
37. J. S. Lee *et al.*, A novel prognostic subtype of human hepatocellular carcinoma derived from hepatic progenitor cells. *Nat. Med.* **12**, 410–416 (2006).
38. S. Cairo *et al.*, Hepatic stem-like phenotype and interplay of Wnt/beta-catenin and Myc signaling in aggressive childhood liver cancer. *Cancer Cell* **14**, 471–484 (2008).
39. J. S. Lee *et al.*, Application of comparative functional genomics to identify best-fit mouse models to study human cancer. *Nat. Genet.* **36**, 1306–1311 (2004).
40. N. Aizarani *et al.*, A human liver cell atlas reveals heterogeneity and epithelial progenitors. *Nature* **572**, 199–204 (2019).
41. L. Zhou *et al.*, Integrated analysis highlights the immunosuppressive role of TREM2(+) macrophages in hepatocellular carcinoma. *Front. Immunol.* **13**, 848367 (2022).
42. Y. Liao, J. Wang, E. J. Jaehnig, Z. Shi, B. Zhang, WebGestalt 2019: Gene set analysis toolkit with revamped UIs and APIs. *Nucleic Acids Res.* **47**, W199–W205 (2019).
43. N. Kiuchi *et al.*, STAT3 is required for the gp130-mediated full activation of the c-myc gene. *J. Exp. Med.* **189**, 63–73 (1999).
44. E. J. Sun, M. Wankell, P. Palamuthusingam, C. McFarlane, L. Hebbard, Targeting the PI3K/Akt/mTOR pathway in hepatocellular carcinoma. *Biomedicines* **9**, 1639 (2021).
45. B. N. Song, I. S. Chu, A gene expression signature of FOXM1 predicts the prognosis of hepatocellular carcinoma. *Exp. Mol. Med.* **50**, e418 (2018).
46. G. S. Yochum, R. Cleland, R. H. Goodman, A genome-wide screen for beta-catenin binding sites identifies a downstream enhancer element that controls c-Myc gene expression. *Mol. Cell Biol.* **28**, 7368–7379 (2008).
47. E. C. Partridge *et al.*, Occupancy maps of 208 chromatin-associated proteins in one human cell type. *Nature* **583**, 720–728 (2020).
48. C. G. A. R. Network, Comprehensive and integrative genomic characterization of hepatocellular carcinoma. *Cell* **169**, 1327–1341.e23 (2017).
49. P. Filippakopoulos *et al.*, Selective inhibition of BET bromodomains. *Nature* **468**, 1067–1073 (2010).
50. M. P. Schwalm, S. Knapp, BET bromodomain inhibitors. *Curr. Opin. Chem. Biol.* **68**, 102148 (2022).
51. S. Hagiwara *et al.*, Activation of JNK and high expression level of CD133 predict a poor response to sorafenib in hepatocellular carcinoma. *Br. J. Cancer* **106**, 1997–2003 (2012).
52. W. Chen *et al.*, Activation of c-Jun predicts a poor response to sorafenib in hepatocellular carcinoma: Preliminary Clinical Evidence. *Sci. Rep.* **6**, 22976 (2016).
53. J. Yu *et al.*, Inhibitory role of peroxisome proliferator-activated receptor gamma in hepatocarcinogenesis in mice and in vitro. *Hepatology* **51**, 2008–2019 (2010).
54. F. X. Schaub *et al.*, Pan-cancer alterations of the MYC oncogene and its proximal network across the Cancer Genome Atlas. *Cell Syst.* **6**, 282–300.e2 (2018).
55. M. Gabay, Y. Li, D. W. Felsher, MYC activation is a hallmark of cancer initiation and maintenance. *Cold Spring Harb. Perspect. Med.* **4**, a014241 (2014).
56. R. Dhanasekaran *et al.*, MYC overexpression drives immune evasion in hepatocellular carcinoma that is reversible through restoration of proinflammatory macrophages. *Cancer Res.* **83**, 626–640 (2023).
57. T. R. Kress *et al.*, Identification of MYC-dependent transcriptional programs in oncogene-addicted liver tumors. *Cancer Res.* **76**, 3463–3472 (2016).
58. B. L. Allen-Petersen, R. C. Sears, Mission possible: Advances in MYC therapeutic targeting in cancer. *BioDrugs* **33**, 539–553 (2019).
59. J. R. Whitfield, L. Soucek, The long journey to bring a Myc inhibitor to the clinic. *J. Cell Biol.* **220**, e202103090 (2021).
60. A. G. Cochran, A. R. Conery, R. J. Sims III, Bromodomains: A new target class for drug development. *Nat. Rev. Drug. Discov.* **18**, 609–628 (2019).
61. E. K. Baker *et al.*, BET inhibitors induce apoptosis through a MYC independent mechanism and synergise with CDK inhibitors to kill osteosarcoma cells. *Sci. Rep.* **5**, 10120 (2015).
62. L. Soucek *et al.*, Modelling Myc inhibition as a cancer therapy. *Nature* **455**, 679–683 (2008).